Organic–Inorganic Hybrid Composites

DOI: 10.1002/anie.201209229

Chemically Exfoliated MoS_2 as Near-Infrared Photothermal Agents**

Stanley S. Chou, Bryan Kaehr,* Jaemyung Kim, Brian M. Foley, Mrinmoy De, Patrick E. Hopkins, Jiaxing Huang, C. Jeffrey Brinker, and Vinayak P. Dravid*

The near-infrared (NIR) window refers to a range of wavelengths (700–1300 nm) in which biological tissues are highly transparent.[1] Consequently, biological imaging and therapy modalities employ light at these wavelengths for the monitoring[1] and triggering[2] of biological events in vitro and in vivo. For instance, photothermal ablation takes advantage of NIR absorbing materials for transducing light into heat.[2] The resultant thermal energy can be used for a number of applications, such as tissue ablation and drug release. Despite the intense interest in NIR photothermal agents, their development has suffered from considerable challenges. In particular, few nanomaterials display the requisite absorption profiles required for NIR photothermal transduction.

The initial development of NIR photothermal agents largely focused on anisotropic gold particles[3] such as nanorods,[2] nanocages,[4] and nanostars.[5] These shapes serve as local plasmon antennas for NIR absorbance, but they are encumbered by complicated syntheses. More importantly, because of the non-equilibrium morphologies, anisotropic gold nanostructures inevitably tend to evolve into spheres upon heating.[5]

Consequently, researchers have begun to investigate the NIR photothermal properties of graphene derivatives such as graphene oxide (GO)[6] and reduced graphene oxide (rGO).[7] The exceptional surface-area-to-mass ratio of these two-dimensional (2D) materials makes them promising photothermal candidates that can be loaded with high cargo concentrations. Previously graphene,[8] rGO,[9] and MoS_2[10] among others[11] have been explored for their use as photodectectors. However, a NIR photocurrent response for mechanically exfoliated MoS_2 phototransistors was negligible.[10] Additionally, the efficacy of GO as a NIR photothermal transducer has been debated,[7a] prompting investigation of rGO, as a 2D nanomaterial with potentially improved NIR absorbance.[7a] Unfortunately, rGO is hydrophobic,[12] and thus requires complex surface modifications to be useful in aqueous environments.[7]

As an alternative to the aforementioned materials, we report the NIR-photothermal properties of chemically exfoliated MoS_2 ($ceMoS_2$). $ceMoS_2$ is a mixed phase, two-dimensional amphiphile that is easy to synthesize in large batches and is directly dispersible in water.[13] Further, the magnitude of its ζ potential (-45 mV, comparable to GO)[14] provides great colloidal stability in aqueous media. We show that owing to an absorbance profile reaching into the NIR, $ceMoS_2$ heats up rapidly upon NIR irradiation. Because of its high surface-area-to-mass ratio, $ceMoS_2$ also possesses loading capacities on par with GO, the current best-in-class.[15] Clearly, $ceMoS_2$ possesses many desirable traits present in the aforementioned photothermal agents.

To synthesize $ceMoS_2$, we use the Morrison method[13a,c] which breaks the weak interlayer forces in bulk MoS_2 through ultrasonication and the formation of H_2 gas. Compared to mechanical exfoliation[16] or vapor-deposited films on wafer templates,[17] the MoS_2 sheets obtained through this method tend to lack the crystallinity required for usage as semiconducting active layers.[13c,18] However, this method renders the resulting sheets water dispersible (they are natively hydrophobic), is scalable, and can be readily adapted for other transition metal dichalcogenides.[13c,19] A typical synthesis produces approximately 300 mL of MoS_2 at a concentration ≥ 300 ppm (see the Experimental Section) and is easily scalable. Physical characterization of the resultant sheets using atomic force microscopy ($n = 100$) revealed mean longest diagonals of 0.80 μm with an average thickness of 1.56 nm ($n = 40$ sheets), which is consistent with a MoS_2

[*] Dr. B. Kaehr, Prof. C. J. Brinker
Advanced Materials Laboratory Sandia National Laboratories
Albuquerque, NM 87106 (USA)
and
Department of Chemical and
Nuclear Engineering Center for Micro-engineered Materials
University of New Mexico, Albuquerque, NM 87106 (USA)
E-mail: bjkaehr@sandia.gov
S. S. Chou, J. Kim, B. M. Foley, Dr. M. De, Prof. J. Huang, Prof. V. P. Dravid
Department of Materials Science and Engineering
International Institute of Nanotechnology
Northwestern University, Evanston, IL 60208 (USA)
E-mail: s-chou@northwestern.edu
Prof. P. E. Hopkins
Department of Mechanical and Aerospace Engineering
University of Virginia, Charlottesville, VA 22904 (USA)

[**] B.K. and C.J.B. acknowledge support from the U.S. Department of Energy (DOE), Office of Science, Office of Basic Energy Sciences (BES), Division of Materials Sciences and Engineering. Sandia National Laboratories is a multi-program laboratory managed and operated by Sandia Corporation, a wholly owned subsidiary of Lockheed Martin Corporation, for the U.S. Department of Energy's National Nuclear Security Administration under contract number DE-AC04-94AL85000. S.C. thanks D.H.S. for a fellowship and Dr. Y. Lin for helpful discussions. V.P.D. acknowledges support by the National Cancer Institute Center for Cancer Nanotechnology Excellence (CCNE) initiative at Northwestern University award number U54A119341. J.H. acknowledges support from the National Science Foundation (DMR CAREER grant number 0955612) and the Alfred P. Sloan Research Foundation.

Supporting information for this article is available on the WWW under http://dx.doi.org/10.1002/anie.201209229.

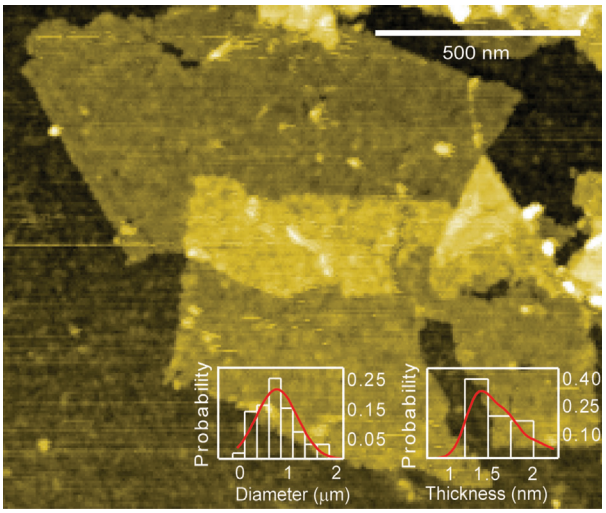

Figure 1. Atomic force microscopy (AFM) micrograph of $ceMoS_2$ sheets. The insets show diameter and thickness profiles.

monolayer[20] (Figure 1 and Figure S1 in the Supporting Information).

NIR absorbance by $ceMoS_2$ was then characterized (Figure 2a). Here, the concentration of $ceMoS_2$ was determined using induction-coupled plasma mass spectroscopy (ICP-MS), which provides parts-per-billion sensitivity (ppb). This enabled the accurate quantification of the $ceMoS_2$ mass extinction coefficient ($\lambda = 800$ nm, $29.2\ L\,g^{-1}\,cm^{-1}$), which represents a $\approx$7.8-fold increase compared to nano-GO ($3.6\ L\,g^{-1}\,cm^{-1}$) and is comparable to nano-rGO ($24.6\ L\,g^{-1}\,cm^{-1}$).[7a] It also represents a two times increase over gold nanorods ($13.9\ L\,g^{-1}\,cm^{-1}$).[7a]

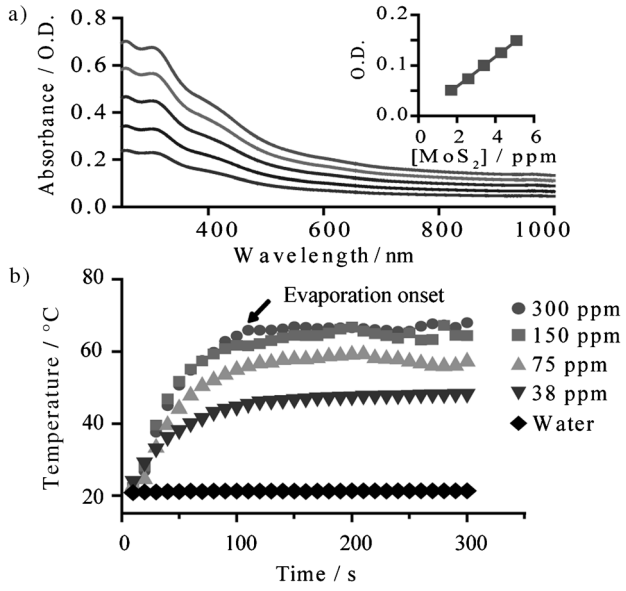

Figure 2. a) Absorbance profile of $ceMoS_2$. The top curve is 5 ppm. Each subsequent curve is 0.5 times diluted. The inset is the Beer's law plot at 800 nm (O.D. = optical density). b) Photothermal heating curves of $ceMoS_2$ across a range of concentrations.

Next, we investigated photothermal heating of solutions of $ceMoS_2$, prepared over a range of concentrations, by irradiation with a continuous wave laser at $\lambda = 800$ nm ($0.8\ W\,cm^{-2}$) and measurement of the solution temperature as a function of time (Figure 2b.). Here, the superior NIR photothermal transduction by $ceMoS_2$ is demonstrated, as we observed solution temperatures above 40°C, the figure of merit for thermal ablation therapy,[21] to be generated with very low concentrations of $ceMoS_2$ (< 38 ppm). This is a marked improvement over GO.[7a] Thus, $ceMoS_2$ combines the NIR heating features of rGO,[7a] with the water dispersibility of GO using a simple and readily scalable batch process. Additionally, x-ray photoelectron spectroscopy (XPS) showed no significant oxidation of as prepared and IR-irradiated $ceMoS_2$ (Figure S2).

To show that $ceMoS_2$, in the absence of NIR irradiation, is otherwise biocompatible, we examined its capability to form non-denaturing host–guest interactions with α-chymotrypsin (ChT), a serine protease. Here, ChT was chosen for its broad bio-sensing applicability and its well documented loading capacity in a wide variety of materials, including gold nanoparticles,[22] polymeric micelles,[23] dendrimers,[24] porphyrins,[25] carbon nanotubes,[26] and GO.[14a,15] As ChT contains a cationic active site that can complex with anionic materials through electrostatic complementation, its loading can be quantified by monitoring enzymatic inhibition by $ceMoS_2$. To investigate ChT loading on $ceMoS_2$, we incubated a range of concentrations of $ceMoS_2$ with 16 μM ChT in 96 well plates. After 30 minutes of incubation, *N*-succinyl-l-phenylalanine-*p*-nitroanilide (SPNA), a chromogenic substrate for measuring ChT activity was added to a final concentration of 2 mM. The data were then fitted using nonlinear regression. From the resulting inhibition curve (Figure 3a), it can be seen that 50% of ChT is inhibited by 5 ppm of $ceMoS_2$. Full inhibition (> 95%) is attained at 11 ppm. This value is significant, as it demonstrates that $ceMoS_2$ has a ChT dose-inhibition capacity comparable to GO, which is the current benchmark material (full comparison in the Supporting Information).[15]

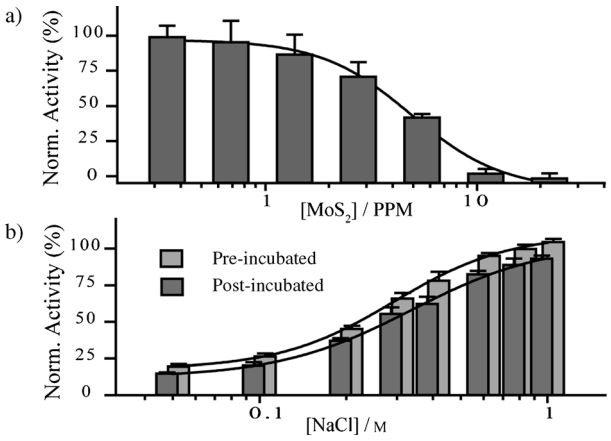

Figure 3. a) Inhibition of ChT using increasing doses of $ceMoS_2$. b) Activity of ChT–$ceMoS_2$ pre-incubated and post-incubated with increasing concentrations of NaCl.

To show that the host–guest interaction between ChT and $ceMoS_2$ is reversible, we incubated ChT with 11 ppm of $ceMoS_2$ (full inhibition concentration) in media of increasing ionic strength to negate electrostatic interactions.[27] In one set of experiments, $ceMoS_2$ was added to ChT in media pre-spiked with NaCl (pre-incubated). In another set of experiments, NaCl was added after first allowing $ceMoS_2$ and ChT to form a complex for 30 minutes (post-incubated). In the case of pre-incubation with NaCl, 100% of ChT activity was observed to be recovered at [NaCl] = 750 mM. Comparatively, only 90% of ChT activity was recovered if NaCl was added after $ceMoS_2$ was allowed to first form a complex with ChT (Figure 3b). Interestingly, the rate of recovery did not change with increased pre-incubation times (24 h, see the Supporting Information). These observations suggest that either some part of ChT is denatured following complexation with $ceMoS_2$, or that there may be a two component complexation process where one component acts through non-electrostatic forces.[15]

To distinguish between these mechanisms, we investigated the protein structure of ChT after complexation with $ceMoS_2$ using circular dichroism (CD) and fluorescence spectroscopy. Here, using CD, it can be seen that native ChT structure presents characteristic minima at 232 and 204 nm (Figure 4a and Figure S3).[15] Upon denaturation (DChT), the minimum at 232 nm diminishes and the minimum at 204 nm intensifies and shifts toward 198 nm (Figure S3). It can also be seen that ChT, once inhibited by complexation with $ceMoS_2$, displays identical CD spectra to free ChT (Figure 4a). In fact, the CD spectra of ChT remained consistent even after 24 h of incubation with $ceMoS_2$, thus indicating complexation does not lead to protein denaturation.

The preservation of the ChT structure was also corroborated by fluorescence spectroscopy. Here, as the secondary structure of ChT unravels, its tryptophan (trp) residue becomes increasingly exposed to water. This causes a red-shift in its fluorescence peak, from 334 to 352 nm (Figure S3).[28] As this shift was not observed with the inhibited ChT–$ceMoS_2$, the fluorescence spectroscopy data corroborates the findings of the CD study (Figure 4b). It is therefore likely that the 90% recovery seen for $ceMoS_2$-complexed ChT post-incubated with NaCl is due to a two-component binding process, with the majority due to electrostatic complementarity, and the remaining (non-recovered) binding due to weak intermolecular forces[15,22] attributable to the amphiphillic properties of $ceMoS_2$.[13b]

The combination of biomolecular friendliness, high protein loading, and favorable photothermal characteristics of $ceMoS_2$ suggests its potential as an effective NIR photothermal agent. To demonstrate this potential, we irradiated aliquots of ChT-complexed $ceMoS_2$ with NIR light for 15 minutes ($\lambda = 800$ nm, 0.8 W cm^{-2}). After treatments, secondary structures of ChT were examined with CD and fluorescence spectroscopy (Figure 4a,b and Figure S3). Residual activity was monitored by spiking samples with NaCl (750 mM) and reversing the ChT–$ceMoS_2$ complexation. The activity of ChT after various treatments is shown in Figure 4c.

In these experiments, it can be seen that the ChT–$ceMoS_2$ complexes irradiated with NIR laser light showed complete denaturation (Figure 4a,b and Figure S3). Further, they show little enzymatic activity (Figure 4c). This demonstrates $ceMoS_2$ as an effective enzymatic receptor capable of selective destruction of its targets through NIR photothermal transduction.

To demonstrate the photothermal ablation therapy for mammalian cells, we then examined its administration in vitro. Here, we collected Hela cells at a concentration of 10^5 mL^{-1}. The solution was then spiked with $ceMoS_2$ to final concentrations of 20 and 40 ppm. These dosages are roughly an order of magnitude lower than those reported in previous GO studies.[6b,29] As with ChT experiments, parallel aliquots were used for controls. All experiments were performed in independent triplicates. After various treatments (irradiated, non-irradiated, with and without $ceMoS_2$), cells were washed with phosphate-buffered saline (PBS; three times) and then incubated in a 96 well plate for 24 hrs (10000/well). Cell viabilities were then measured using Celltiter 96 (Promega), a negatively charged, water-soluble MTT agent that does not interfere with cell activity measurements.[12]

As shown in Figure 5, cells treated with $ceMoS_2$ and NIR irradiation ($\lambda = 800$ nm, 20 minutes) show zero viability at both $ceMoS_2$ concentrations. This is not surprising as solution temperatures reached 57 and 64 °C, respectively, well above thermal ablation thresholds. Optical micrographs of the treated cells confirm the Celltiter results (Figure S4). This

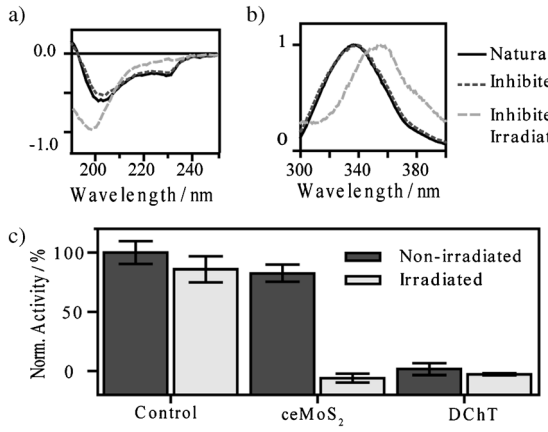

Figure 4. a) Normalized CD and b) fluorescent spectra of select ChT samples after various treatments. A full set of samples is available in the Supporting Information (Norm. = normalized intensity). c) Normalized activity assay of $ceMoS_2$-ChT or decoupled ChT in 750 mM NaCl after various treatments.

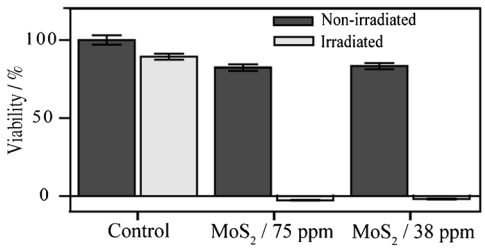

Figure 5. Hela cell viabilities after various treatments.

presents a stark contrast to cells treated with $ceMoS_2$ without irradiation. There, cell viabilities of 82 and 81% were observed. It is thus consistent with previous reports showing MoS_2 materials to be relatively non-toxic to cells.[30] Cells irradiated with NIR without $ceMoS_2$ showed a viability of 89%. This observation shows that the photothermal process of $ceMoS_2$ can be extended for cellular destruction.

As the cellular viability is closely related to the temperature rise induced from the $ceMoS_2$ photothermal transduction, we examined the physical processes driving the temperature rise in the cellular matrix by measuring the rate of heat transfer from the $ceMoS_2$ into an aqueous medium with time-domain thermo-transmission (TDTT).[31] TDTT has been used previously by several groups to quantify the thermal boundary conductance[32] between nanosystems suspended in elastically softer media.[31,33] In short, TDTT uses a brief laser pulse to heat the optically absorbing $ceMoS_2$ while a time-delayed probe pulse monitors the temperature change of the $ceMoS_2$. The thermal decay of the $ceMoS_2$ over several nanoseconds is related to the heat flow from the $ceMoS_2$ to the surrounding media, as described in detail elsewhere.[34,35] For our specific TDTT experiments, we measured the thermal decay of 30 ppm of $ceMoS_2$ suspended in deionized water. We monitored the temperature decay at 800 nm to directly mimic the previously described experiments and find the thermal boundary conductance from the $ceMoS_2$ to its surrounding to be $(77.5 \pm 9)\ MW\,m^{-2}\,K^{-1}$. To put this into perspective, this is comparable to the interfacial heat transfer between two solids[36] or between carbon nanotubes and water.[31,33b] This relatively low resistance (high conductance) offers an equivalent resistance of about 10 nm of a typical mammalian cell matrix (assuming a cytoplasmic water content of 70%), indicating the high efficacy of thermal coupling between the $ceMoS_2$ and the surrounding media. Using this measured value of thermal boundary conductance, from steady-state heat transfer theory[34,37] we calculate a 30 K temperature rise in the intracellular medium for a 30 ppm $ceMoS_2$ suspensions irradiated at $\lambda = 800$ nm ($0.8\ W\,cm^{-2}$).

In summary, we have described the optical and photothermal properties of $ceMoS_2$ and report its effectiveness as a NIR photothermal agent. $ceMoS_2$ displays approximately 7.8 times greater absorbance in the NIR relative to GO, with an extinction coefficient at 800 nm of $29.2\ L\,g^{-1}\,cm^{-1}$, which is higher than that of gold nanorods ($13.9\ L\,g^{-1}\,cm^{-1}$) and is comparable to rGO ($24.6\ L\,g^{-1}\,cm^{-1}$).[7a] Unlike the hydrophobic rGO, however, $ceMoS_2$ is also directly water dispersible after exfoliation, and easily purified (dialysis under water flow). It also possesses an enhanced biomolecular protein loading capacity comparable to GO, the current best-in-class material.[15] These characteristics provide a foundation to explore the use of $ceMoS_2$ for a wide range of biological applications and beyond (e.g., solar paints and coatings), where broad light absorption into the NIR is desirable.

Experimental Section

Synthesis of $ceMoS_2$: Procedures were adapted from Joensen et al.[16] In a nitrogen environment, ≈350 mg of MoS_2 powder was immersed in ≈3.5 mL of *n*-butyllithium (1.6 M in hexane) and stirred for 48 h. Mixture was then filtered over Whatman #41 filter and rinsed with 100 mL of hexane. To the semi-dry mixture, 300 mL of H_2O (18.2 MΩ cm at 25 °C) was added. The mixture was sonicated for 1 h to achieve exfoliation. The MoS_2 nanosheets were then centrifuged and washed with H_2O five times. It was then collected and dialyzed against H_2O for 5 days. The concentration was determined by ICP-MS.

Additional experimental details are provided in the Supporting Information.

Received: November 17, 2012
Revised: February 14, 2013
Published online: March 7, 2013

Keywords: dichalcogenides · molybdenum · organic–inorganic hybrid composites · photothermal therapy · supramolecular chemistry

[1] F. F. Jöbsis-vanderVliet, *J. Biomed. Opt.* **1999**, *4*, 392 – 396.
[2] X. Huang, I. H. El-Sayed, W. Qian, M. A. El-Sayed, *J. Am. Chem. Soc.* **2006**, *128*, 2115 – 2120.
[3] W. Zhao, J. M. Karp, *Nat. Mater.* **2009**, *8*, 453 – 454.
[4] S. E. Skrabalak, J. Chen, Y. Sun, X. Lu, L. Au, C. M. Cobley, Y. Xia, *Acc. Chem. Res.* **2008**, *41*, 1587 – 1595.
[5] J. Xie, J. Y. Lee, D. I. C. Wang, *Chem. Mater.* **2007**, *19*, 2823 – 2830.
[6] a) B. Tian, C. Wang, S. Zhang, L. Feng, Z. Liu, *ACS Nano* **2011**, *5*, 7000 – 7009; b) K. Yang, S. Zhang, G. Zhang, X. Sun, S.-T. Lee, Z. Liu, *Nano Lett.* **2010**, *10*, 3318 – 3323.
[7] a) J. T. Robinson, S. M. Tabakman, Y. Liang, H. Wang, H. Sanchez Casalongue, D. Vinh, H. Dai, *J. Am. Chem. Soc.* **2011**, *133*, 6825 – 6831; b) K. Yang, J. Wan, S. Zhang, B. Tian, Y. Zhang, Z. Liu, *Biomaterials* **2012**, *33*, 2206 – 2214.
[8] F. Xia, T. Mueller, Y.-m. Lin, A. Valdes-Garcia, P. Avouris, *Nat. Nanotechnol.* **2009**, *4*, 839 – 843.
[9] a) H. Chang, Z. Sun, Q. Yuan, F. Ding, X. Tao, F. Yan, Z. Zheng, *Adv. Mater.* **2010**, *22*, 4872 – 4876; b) B. Chitara, L. S. Panchakarla, S. B. Krupanidhi, C. N. R. Rao, *Adv. Mater.* **2011**, *23*, 5419 – 5424.
[10] Z. Yin, H. Li, H. Li, L. Jiang, Y. Shi, Y. Sun, G. Lu, Q. Zhang, X. Chen, H. Zhang, *ACS Nano* **2012**, *6*, 74 – 80.
[11] C. N. R. Rao, H. S. S. R. Matte, K. S. Subrahmanyam, *Acc. Chem. Res.* **2013**, *46*, 149 – 159.
[12] K.-H. Liao, Y.-S. Lin, C. W. Macosko, C. L. Haynes, *ACS Appl. Mater. Interfaces* **2011**, *3*, 2607 – 2615.
[13] a) P. Joensen, R. F. Frindt, S. R. Morrison, *Mater. Res. Bull.* **1986**, *21*, 457 – 461; b) W. M. R. Divigalpitiya, R. F. Frindt, S. R. Morrison, *Science* **1989**, *246*, 369 – 371; c) G. Eda, H. Yamaguchi, D. Voiry, T. Fujita, M. Chen, M. Chhowalla, *Nano Lett.* **2011**, *11*, 5111 – 5116.
[14] a) S. S. Chou, M. De, J. Luo, V. M. Rotello, J. Huang, V. P. Dravid, *J. Am. Chem. Soc.* **2012**, *134*, 16725—16733; b) J. Luo, L. J. Cote, V. C. Tung, A. T. L. Tan, P. E. Goins, J. Wu, J. Huang, *J. Am. Chem. Soc.* **2010**, *132*, 17667 – 17669.
[15] M. De, S. S. Chou, V. P. Dravid, *J. Am. Chem. Soc.* **2011**, *133*, 17524 – 17527.
[16] a) B. Radisavljevic, A. Radenovic, J. Brivio, V. Giacometti, A. Kis, *Nat. Nanotechnol.* **2011**, *6*, 147 – 150; b) H. S. S. Ramakrishna Matte, A. Gomathi, A. K. Manna, D. J. Late, R. Datta, S. K. Pati, C. N. R. Rao, *Angew. Chem.* **2010**, *122*, 4153 – 4156; *Angew. Chem. Int. Ed.* **2010**, *49*, 4059 – 4062.
[17] a) K.-K. Liu, W. Zhang, Y.-H. Lee, Y.-C. Lin, M.-T. Chang, C.-Y. Su, C.-S. Chang, H. Li, Y. Shi, H. Zhang, C.-S. Lai, L.-J. Li, *Nano Lett.* **2012**, *12*, 1538 – 1544; b) Y.-H. Lee, X.-Q. Zhang, W. Zhang,

M.-T. Chang, C.-T. Lin, K.-D. Chang, Y.-C. Yu, J. T.-W. Wang, C.-S. Chang, L.-J. Li, T.-W. Lin, *Adv. Mater.* **2012**, *24*, 2320 – 2325.
[18] P. Joensen, E. D. Crozier, N. Alberding, R. F. Frindt, *J. Phys. C* **1987**, *20*, 4043.
[19] Z. Zeng, Z. Yin, X. Huang, H. Li, Q. He, G. Lu, F. Boey, H. Zhang, *Angew. Chem.* **2011**, *123*, 11289 – 11293; *Angew. Chem. Int. Ed.* **2011**, *50*, 11093 – 11097.
[20] D. J. Late, B. Liu, H. S. S. R. Matte, C. N. R. Rao, V. P. Dravid, *Adv. Funct. Mater.* **2012**, *22*, 1894 – 1905.
[21] a) H.-C. Huang, K. Rege, J. J. Heys, *ACS Nano* **2010**, *4*, 2892 – 2900; b) X. Huang, P. K. Jain, I. H. El-Sayed, M. A. El-Sayed, *Photochem. Photobiol.* **2006**, *82*, 412 – 417; c) J. Overgaard, *Int. J. Radiat. Oncol. Biol. Phys.* **1989**, *16*, 535 – 549.
[22] N. O. Fischer, C. M. McIntosh, J. M. Simard, V. M. Rotello, *Proc. Natl. Acad. Sci. USA* **2002**, *99*, 5018 – 5023.
[23] B. S. Sandanaraj, D. R. Vutukuri, J. M. Simard, A. Klaikherd, R. Hong, V. M. Rotello, S. Thayumanavan, *J. Am. Chem. Soc.* **2005**, *127*, 10693 – 10698.
[24] F. Chiba, T.-C. Hu, L. J. Twyman, M. Wagstaff, *Chem. Commun.* **2008**, 4351 – 4353.
[25] K. Kano, Y. Ishida, *Chem. Asian J.* **2008**, *3*, 678 – 686.
[26] B. Zhang, Y. Xing, Z. Li, H. Zhou, Q. Mu, B. Yan, *Nano Lett.* **2009**, *9*, 2280 – 2284.
[27] A. Verma, J. M. Simard, V. M. Rotello, *Langmuir* **2004**, *20*, 4178 – 4181.
[28] a) A. S. Ladokhin, *Encyclopedia of Analytical Chemistry*, Wiley, Hoboken, **2006**; b) N. O. Fischer, A. Verma, C. M. Goodman, J. M. Simard, V. M. Rotello, *J. Am. Chem. Soc.* **2003**, *125*, 13387 – 13391.
[29] Note: Value calculated from reference [7b] using the reported dose (20 mg kg^{-1}) by assuming a typical mouse weight of 250 g and a blood volume of 1.5 mL.
[30] H. Wu, R. Yang, B. Song, Q. Han, J. Li, Y. Zhang, Y. Fang, R. Tenne, C. Wang, *ACS Nano* **2011**, *5*, 1276 – 1281.
[31] S. T. Huxtable, D. G. Cahill, S. Shenogin, L. Xue, R. Ozisik, P. Barone, M. Usrey, M. S. Strano, G. Siddons, M. Shim, P. Keblinski, *Nat. Mater.* **2003**, *2*, 731 – 734.
[32] E. T. Swartz, R. O. Pohl, *Rev. Mod. Phys.* **1989**, *61*, 605 – 668.
[33] a) S. T. Huxtable, D. G. Cahill, S. Shenogin, P. Keblinski, *Chem. Phys. Lett.* **2005**, *407*, 129 – 134; b) S. D. Kang, S. C. Lim, E.-S. Lee, Y. W. Cho, Y.-H. Kim, H.-K. Lyeo, Y. H. Lee, *ACS Nano* **2012**, *6*, 3853 – 3860.
[34] D. G. Cahill, *Rev. Sci. Instrum.* **2004**, *75*, 5119 – 5122.
[35] a) P. E. Hopkins, J. R. Serrano, L. M. Phinney, S. P. Kearney, T. W. Grasser, C. T. Harris, *J. Heat Transfer* **2010**, *132*, 081302; b) A. J. Schmidt, X. Chen, G. Chen, *Rev. Sci. Instrum.* **2008**, *79*, 114902.
[36] E. Pop, *Nano Res.* **2010**, *3*, 147 – 169.
[37] D.-W. Oh, C. Ko, S. Ramanathan, D. G. Cahill, *Appl. Phys. Lett.* **2010**, *96*, 151906.

